

Pressure driven transport of neutral macro-solute in microchannel with porous wall at high surface potential

Sourav Mondal^{a,b} and Sirshendu De^{a*}

^a *Department of Chemical Engineering, Indian Institute of Technology Kharagpur,
Kharagpur 721302, India*

^b *Mathematical Institute, University of Oxford, Oxford OX2 6GG, UK*

Journal accepted: International Journal of Heat and Mass Transfer

Date of acceptance: 27 Aug 2016

DOI: 10.1016/j.ijheatmasstransfer.2016.08.092

Full citation information:

Sourav Mondal, Sirshendu De, Pressure driven transport of neutral macro-solute in microchannel with porous wall at high surface potential, International Journal of Heat and Mass Transfer, Volume 104, January 2017, Pages 574-583, ISSN 0017-9310, <http://dx.doi.org/10.1016/j.ijheatmasstransfer.2016.08.092>.

* corresponding author

Phone: +91-3222-283926

Fax: +91-3222-255303

email: sde@che.iitkgp.ernet.in

Abstract

Mass transport of macro-solutes under streaming potential in a microchannel with porous wall is presented in this study. The streaming field under high wall potential and overlapping electric double layer with coupled velocity and concentration of neutral solutes is computed numerically in this work. Streaming potential increases by 7 folds as κH decreases from 0.7 to 0.1 at $\zeta = -50$ mV, where, κ^{-1} is Debye length, H is channel half height and ζ is wall zeta potential. Mass transport in terms of Sherwood number is calculated including osmotic effect of the solution and selective retention of macrosolutes. Electroviscous effects resulting from streaming potential and overlapping electric double layer at higher wall zeta potential have significant effect on velocity field and the mass transport of macrosolutes. Apparent viscosity due to this effect increases upto 3.2 times the solution viscosity at $\kappa H = 0.2$ for $\zeta = -50$ mV. This effect is intensified upto 4 times at higher wall potential, $\zeta = -200$ mV at $\kappa H = 0.5$. At these points, the velocity profile suffers the most adversely affecting the mass transfer reducing Sherwood number to 4 (about 5 times reduction compared to higher κH) at $\zeta = -200$ mV and $\kappa H = 0.5$. Sherwood number reduces by three to four folds at the critical κH values, representing the minimum. The induced electrical field due to the streaming potential is higher compared to axial pressure drop for $|\zeta| > 50$ mV at $\kappa H < 0.3$. The electric double layer overlaps for the values of κH upto 0.7 corresponding to $\zeta = -50$ mV. In case of high ζ (-200 mV), the centerline potential can be as high as 75% of the wall potential for $\kappa H = 1.5$. The minimum wall Peclet number ($\overline{Pe_w}$) occurs at $\kappa H = 0.5$ for $\zeta = -200$ mV, which is five times less than the situation without electrokinetic effects.

Keywords: Microchannel; overlapping electric double layer; streaming potential; species transport; porous wall

1.0 Introduction

Flow through microchannels under the influence of electrokinetic effects is a promising area of research [1, 2]. The transport phenomena associated with electrokinetic flow in microchannels is useful to quantify microscale heat and mass transfer. Fluid flow combined with heat transfer has been studied by various researchers in microscale heat exchanger [3], micro-chip cooling [4], micro-electronic-mechanical-systems (MEMS) [5], microreactors [6], etc. The corresponding mass transport problem has applications in transdermal drug delivery [7, 8], electrolyte transport in fuel cells [9], transport in hydrogel [10], etc.

Typically, the electrokinetic flow in microchannel can be categorized in four different regimes: electroosmosis, electrophoresis, flow due to streaming field and sedimentation potential. Electroosmosis and electrophoresis occur only in presence of electric field and can occur in conjugation with the pressure gradient. Mass transport in electro kinetically actuated pressure driven flow has already been theoretically analyzed for rectangular channels [11]. The semi-analytical solution approach quantifies the solute transport and dispersion for small zeta potential varying in x and y dimensions. Solute transport in microchannels can also be affected by surface reaction or adsorption which can occur during DNA hybridization or catalytic reaction in micro-reactors [12, 13]. The dynamics of chemical reaction as well as adsorption affecting the solute transport was studied. The different regimes of diffusion controlled or reaction kinetics controlled or adsorption dominant are also identified based on the system configuration and operating conditions. In the absence of external field, the streaming field and sedimentation potential are both generated due to the advection of the mobile counterions by non-electrical forces. The mass transport associated with such electrokinetic flows can be augmented by changing the electrolyte concentration, dimensions

of the channel, and tuning the surface potential of the channel walls. In case of flow due to the streaming field, the overall flow is hindered by the conduction current, which is manifested in apparent increase in viscosity of the fluid, recognized as the electroviscous effects [14-17]. Impact of the electroviscous effects results in reduced efficiency of the system, as reported by Wang et al., [18] in the case of nanofluidic channels. However, the above mentioned studies deal with microchannels with impervious walls.

Electrokinetic flow in microchannels with porous walls has potential application in electrokinetic transport and separation of biomolecules [19], microfluidic separation systems [20], basic clinical diagnostics [21], etc. However, studies on mass transport in microchannel are mostly limited to quantification of dispersion of micro-solutes (electrolytes) [22-24], in an impermeable conduit. Few reports are available for studies on mass transport of neutral macrosolute across the porous wall in a microchannel. De and coworkers recently reported mass transport of neutral solutes in a microchannel with porous wall under the combined action of Poiseuille flow and external electric field [25-28]. There has been a recent analytical study on the shear dispersion of the neutral solutes by electroosmotic flow in a microchannel and microtube with porous walls by Dejam et al. [29, 30]. They have used Reynolds decomposition technique to solve for the coupled flow-species system. A 1D diffusion dominated species transport equation in the porous medium has been prescribed instead of the interface mixed boundary condition. The shear dispersion coefficient depends on the Debye-Hückel parameter, Poiseuille contribution fraction and Péclet number. However, this study is limited to the Debye-Hückel approximation ($|\zeta| < 25$ mV) and does not consider the effects of streaming potential. There is a report by Zhao et al., on the streaming potential analysis in case of parallel plate impervious channel, again in the limit of small wall potentials [31]. However, a numerically intensive study on the electroviscous effects at high surface potentials (well beyond the Debye-Hückel limit) has been reported recently [32]. This

work extends the analysis for the case of soft deformable periodic channel walls. However, this work is restricted to electro-hydrodynamics and do not explore the species transport particularly through porous walls of the walls. Mondal and De have already worked on this problem of species transport through porous channel walls in presence of streaming potential for low wall potential [33].

The ionic potential distribution around a charged interface due to the formation of the electrical double layer (EDL) is represented mathematically by the Poisson-Boltzmann equation (PBE). Three fundamental underlying assumptions are inherent in the PBE: (i) continuum framework of the electrolyte medium; (b) ignoring the steric effects of the ions, considering them to be point charges and (c) the non-mean field electrostatic interactions are absent, ions responds only to the ensemble-averaged field magnitude. The PBE for $z:z$ symmetric solute is simplified using the Debye-Hückel limit for low surface potential ($|\zeta| < 25$ mV). However, there are several situations where the surface potential is high ($|\zeta| \gg 25$ mV) which not only limits the application of Debye-Hückel approximation but leads to overlapped EDL and consequent localized distribution of cation and anion within the EDL [34]. In the present study, the effects of overlapped EDL at high wall potential are computed along with the ionic distribution across the microchannel. The effect of the overlapped EDL together with streaming field is reflected in the velocity profile. Potential distribution and concentration field are solved numerically taking into account the wall permeability and selective transport of macrosolutes. The variation of the system performance in terms of the Sherwood number, permeation rate and permeate concentration, with Debye layer thickness for different values of zeta potential is quantified.

2.0 Mathematical formulation

The co-ordinate system along with the flow behaviour in the microchannel under the combined pressure gradient and electro-osmotic condition under streaming potential is illustrated in the schematic shown in Fig. 1. The ionic solution induces a streaming field due to ion advection and opposes the overall electroosmotic flow that affects the corresponding transport of macro-solutes through the walls. The electrolytic solution develops an adjacent electric double layer (EDL) to the channel wall. The followings assumptions are considered: (a) fluid is Newtonian and incompressible; (b) velocity field is laminar and steady state; (c) physical and thermo physical properties are constant; (d) flow is fully developed hydro dynamically; (e) wall zeta potential is constant; (f) electrolyte is symmetric; (g) ions are point charges and do not interact with channel walls; (h) permittivity of fluid is constant and not affected by overall field strength; (i) there is no specific adsorption of electrolytes by the surface and they dissociates completely in solution; (j) there is no particle to wall interaction of the uncharged macrosolute. The Poisson equation describing the electric potential distribution (ψ) due to presence of EDL and ionic concentration is [35],

$$\frac{d^2\psi}{dy^2} = -\frac{ze}{\varepsilon_r\varepsilon_0} \left[n_+^0 \exp\left(\frac{ze}{k_bT}(\psi_c - \psi)\right) - n_-^0 \exp\left(-\frac{ze}{k_bT}(\psi_c - \psi)\right) \right] \quad (1)$$

where, ψ_c , n_+^0 and n_-^0 are the centre line EDL potential, cation and anion number concentration respectively; k_b and T are the Boltzmann constant and temperature in Kelvin, respectively; $\varepsilon_r\varepsilon_0$ represents the dielectric permittivity of the medium and ze is the total electrolytic charge per unit molar concentration. The relevant boundary conditions are,

$$\text{at } y = 0, \quad \frac{d\psi}{dy} = 0 \quad (2a)$$

$$\text{at } y = H, \quad \psi = \zeta \quad (2b)$$

where, H is the half height of the channel and ζ is the wall potential. The number concentration of ions is represented by the Nernst equation as [35],

$$n_{\pm} = n_{\pm}^0 \exp\left(\pm \frac{ze}{k_b T} (\psi_c - \psi)\right) \quad (3)$$

It may be noted that according to the assumption (d), Eq. (3) is valid [36].

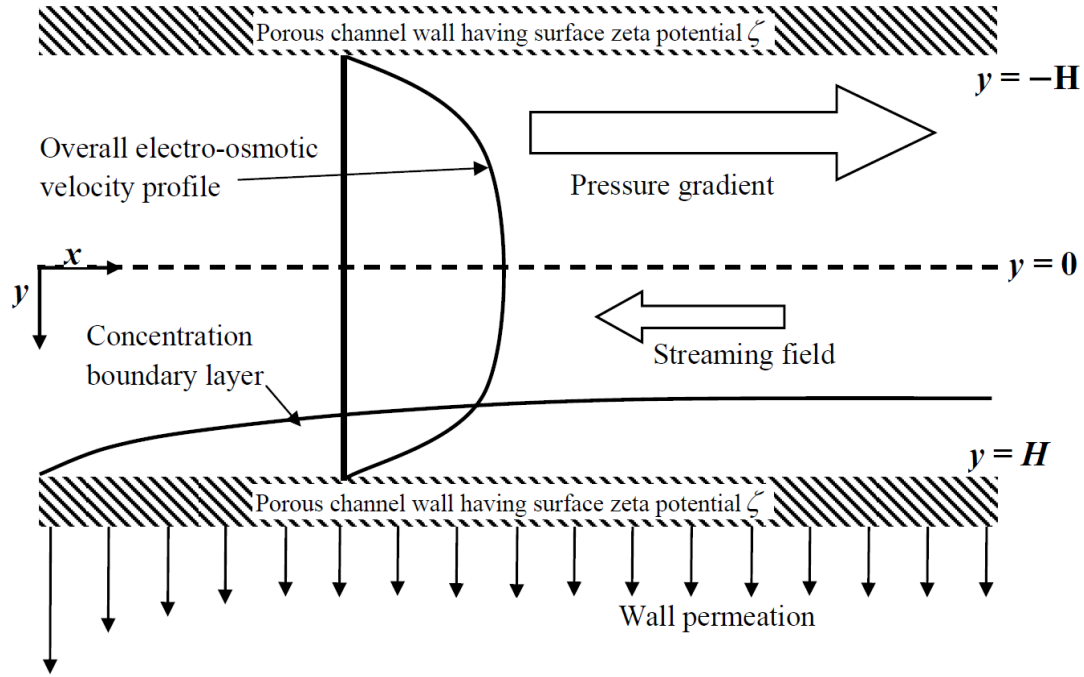


Fig. 1: Schematic representation of the flow profile and concentration boundary layer inside the channel (*Reproduced with permission from John Wiley and Sons*)

2.1 Mass conservation analysis for the ion concentration

Following the derivation from Healy and White [34], the surface charge density (σ_0) can be computed as,

$$\frac{\sigma_0}{e} = \frac{N_s \delta \sinh(\psi_N^* - \alpha)}{1 + \delta \cosh(\psi_N^* - \alpha)} \quad (4)$$

where, $\alpha = \frac{ze\zeta}{k_B T}$ is the non-dimensional surface potential, N_s is the site density of the charged surface, equivalent to 5×10^{18} sites/m² for an oxide surface, ψ_N^* is the Nernst potential expressed in non-dimensional form [35],

$$\psi_N^* = 2.303(pH_{zpc} - pH) \quad (5)$$

where, pH_{zpc} is the pH at which the charged surface is neutral and the δ is the parameter defined as,

$$\delta = 2 \times 10^{-\Delta pK/2} \quad (6)$$

where, ΔpK is the dissociation constant difference. The electrolyte solution is considered as aqueous KCl solution. Hence, the cations in the solution include K^+ and H_3O^+ ions, and anions include Cl^- and OH^- ions. They satisfy the following conservation equations -

$$\int_0^H n_+ dy = \int_0^H n_{K^+} dy + \int_0^H n_{H_3O^+} dy \quad (7)$$

$$\int_0^H n_- dy = \int_0^H n_{Cl^-} dy + \int_0^H n_{OH^-} dy \quad (8)$$

The equilibrium concentration of the H_3O^+ and OH^- ions are related to the dissociation constant of water ($K_w = n_{H_3O^+} \cdot n_{OH^-} = 10^{-14}$), which can be represented in terms of the solution pH as,

$$n_{H_3O^+}^0 = 10^{-pH} \quad (9)$$

$$\text{and, } n_{OH^-}^0 = 10^{pH-14} \quad (10)$$

However, when the electrolyte is in contact with the charged channel wall, OH^- concentration decreases due to adsorption on the solid surface. In order to facilitate equilibrium, a certain amount of water molecules will dissociate into H_3O^+ and OH^- ions as,



Hence, the final concentration of the ions can be presented as:

$$\int_0^H n_{\text{H}_3\text{O}^+} dy = \overline{n_{\text{H}_3\text{O}^+}} H = n_{\text{H}_3\text{O}^+}^0 H + N_d \quad (12)$$

$$\int_0^H n_{\text{OH}^-} dy = \overline{n_{\text{OH}^-}} H = n_{\text{OH}^-}^0 H - \frac{\sigma_0}{e} + N_d \quad (13)$$

where, N_d is the number of water molecules dissociated into H_3O^+ and OH^- . At equilibrium,

$\overline{n_{\text{H}_3\text{O}^+}}$ and $\overline{n_{\text{OH}^-}}$ satisfy the equilibrium relation with respect to dissociation constant of

water $\left(K_w = \overline{n_{\text{H}_3\text{O}^+}} \cdot \overline{n_{\text{OH}^-}} = 10^{-14}\right)$. Now, the above two equations can be solved for

$\overline{n_{\text{H}_3\text{O}^+}}$ and $\overline{n_{\text{OH}^-}}$ corresponding to a particular pH . Assuming that there is no specific

adsorption of KCl ions on the surface and all K^+ and Cl^- ions are in the solution, from Eq.

(7) and Eq. (8) we get,

$$\int_0^H n_+ dy = n_+^0 H + \overline{n_{\text{H}_3\text{O}^+}} H \quad (14)$$

$$\int_0^H n_- dy = n_-^0 H + \overline{n_{\text{OH}^-}} H \quad (15)$$

Therefore, the values of n_-^0 and n_+^0 are obtained by integration of Eq. (3) and are written as:

$$n_-^0 = \frac{\int_0^H n_- dy}{\int_0^H \exp\left(-\frac{ze}{k_b T} [\psi_c - \psi]\right) dy} \quad (16)$$

$$n_+^0 = \frac{\int_0^H n_+ dy}{\int_0^H \exp\left(\frac{ze}{k_b T} [\psi_c - \psi]\right) dy} \quad (17)$$

Thus, the values of ψ_c , n_+^0 and n_-^0 can be solved iteratively using Eqs. (1), (16), (17) for a particular κH . The detailed calculation steps are reported elsewhere [36].

2.2 Streaming field

The effect of the pressure gradient causes mobility of the EDL, which sets up an electric current known as streaming current (I_{str}), to flow in the direction of the imposed fluid motion. The resulting accumulation of the ions in the downstream section of the channel sets up its own electric field (streaming field), which generates the conduction current (I_{cond}), that flows back against the direction of the pressure-driven flow. Thus, the net ionic current (I_{ionic}) is the combination of the streaming current and conduction current [27]. Hence,

$$I_{ionic} = I_{str} + I_{cond} \quad (18)$$

Assuming a z:z symmetric electrolyte, the streaming current can be quantified as [27],

$$I_{str} = ez \int_{-H}^H (n_+ - n_-) u dy \quad (19)$$

where, n_{\pm} are the number concentration of the positive/negative ions, which are represented by Eq. (3). The steady state fully developed velocity field (u) is thus the summation of the poiseuille and opposing streaming-field-induced electroosmotic flow.

$$u(y) = \frac{1}{2\mu} p_x (H^2 - y^2) - \frac{\varepsilon \zeta E_{st}}{\mu} \left(1 - \frac{\psi}{\zeta} \right) \quad (20)$$

where, $p_x = -\frac{dP}{dx}$ and E_{st} is the streaming field. The conduction current in Eq. (18) arises

from the streaming potential developed due to the migration of ions and is expressed as [27],

$$I_{cond} = e \int_{-H}^H \left(n_+ z_+ u_{cond}^+ + n_- z_- u_{cond}^- \right) dy \quad (21)$$

where, the minus (-) and plus (+) signs represent the anion and cation velocities. The conduction velocities (u_{cond}^\pm) are quantified by using a force balance between the frictional drag and the electrical field strength due to streaming potential.

$$u_{cond}^\pm = \frac{z_\pm e E_{st}}{6\pi\mu r^\pm} \quad (22)$$

The anionic and cationic radii are considered to be approximately equal (around 1.5 \AA) to avoid mathematical complexity, $r^+ = r^- = r_{ion}$.

In case of purely pressure driven flow, the net current is zero at steady state ($I_{ionic} = 0$). Using this condition, the streaming field is calculated using Eqs. (18-22) as [27],

$$E_{St} = \frac{\frac{1}{2\mu} p_x \int_{-H}^H (H^2 - y^2) \left[n_+^0 \exp\left(\frac{ze}{k_B T} (\psi - \psi_C)\right) - n_-^0 \exp\left(-\frac{ze}{k_B T} (\psi - \psi_C)\right) \right] dy}{\frac{1}{6\pi\mu r_{ion}} \int_{-H}^H \left[n_+^0 \exp\left(\frac{ze}{k_B T} (\psi - \psi_C)\right) + n_-^0 \exp\left(-\frac{ze}{k_B T} (\psi - \psi_C)\right) \right] dy + \frac{\varepsilon \zeta}{\mu} \int_{-H}^H \left(1 - \frac{\psi}{\zeta} \right) \left[n_+^0 \exp\left(\frac{ze}{k_B T} (\psi - \psi_C)\right) - n_-^0 \exp\left(-\frac{ze}{k_B T} (\psi - \psi_C)\right) \right] dy} \quad (23)$$

The above expression has to be computed numerically to obtain the streaming electric field.

Note that in case of low surface potential, it can be simplified using the Debye-Hückel approximation to obtain an analytical solution [33].

2.3 Solute transport

The velocity profile in microchannel is expressed by Eq. (20). The transport of macro-solutes (neutral) within the mass transfer boundary layer, ignoring electrical and colloidal interaction of the solutes with the channel or electrolyte, is expressed as [22],

$$\vec{v} \cdot \vec{\nabla} c = \vec{\nabla} \cdot (D \vec{\nabla} c) \quad (24)$$

where, c is the concentration of the neutral macro-solute, \vec{v} is the velocity field (u, v) and D is the diffusivity of macro-solute. Eq. (24) can be represented in 2D Cartesian form as,

$$u \frac{\partial c}{\partial x} + v \frac{\partial c}{\partial y} = D \left(\frac{\partial^2 c}{\partial x^2} + \frac{\partial^2 c}{\partial y^2} \right) \quad (24.1)$$

Since, the mass transfer boundary layer is thin in comparison to the channel size, the y -component velocity (v) is approximately equal to the permeation velocity at the wall (v_w), i.e., $v \approx v_w(x)$ [38]. It is important to note that there exists a possibility of deformation of the EDL due to v_w , but the magnitude of the v -component (in the order of 10^{-3} mm/s), causes hardly any significant change within mass transfer boundary layer. However, such effects can be prominent in case of high permeation rate.

Assuming constant diffusivity and applying the lubrication approximation (neglecting $\frac{\partial^2 c}{\partial x^2}$ term) in Eq. (24.1), is simplified as,

$$u \frac{\partial c}{\partial x} + v_w \frac{\partial c}{\partial y} = D \frac{\partial^2 c}{\partial y^2} \quad (25)$$

The relevant boundary conditions are,

$$\text{at } x = 0; c = c_0 \quad (26)$$

$$\text{at } y = H; v_w (c - c_p) + D \frac{\partial c}{\partial y} = 0 \quad (27)$$

$$\text{at } y = 0; c = c_0 \quad (28)$$

where, c_0 is the inlet (and bulk) concentration of the macro-solute and c_p is the permeate side concentration of the macrosolute. The solvent flux across the porous wall (v_w) is computed using Darcy's Law [39] as,

$$v_w = L_p \Delta P_w \left(1 - \frac{\Delta \Pi}{\Delta P_w} \right) \quad (29)$$

where, L_p is the wall permeability and ΔP_w is the average pressure drop across the wall (pressure difference between the wall and permeate side). The osmotic pressure difference, $\Delta \Pi$, arises due to the concentration gradient of the transported solute across the feed and permeate side. The pore size distribution and geometrical factors are all taken care within a lumped parameter i.e., the wall permeability (L_p) [40].

A power law dependence with concentration is considered for computing the osmotic pressure as it represents a generic type valid over a wide range of neutral solutes [41, 42],

$$\Pi(c) = \alpha_1 c^{\alpha_2} \quad (30)$$

Thus, $\Delta \Pi$ is calculated as,

$$\Delta \Pi = \Pi(c_w) - \Pi(c_p) = \alpha_1 c_w^{\alpha_2} \left[1 - (1 - R_r)^{\alpha_2} \right] \quad (31)$$

where, α_1 and α_2 are the constant coefficients, $R_r (= 1 - \frac{c_p}{c_w})$ is wall retention factor which can

be treated as constant specific to the solute [43] and c_w is wall concentration of solute. However, the wall retention factor (R_r) can be computed based on the functions of the pore geometry and size distribution and incorporated in the present analysis, adding mathematical complexity at the cost of marginal improvement in accuracy.

It must be stated here, that the wall is considered to be completely permeable to the electrolytes, but selectively permeable to macrosolutes. Thus Eq. (25) is solved implicitly using Eqs. (20, 29 and 31). Note that Eq. (28) is coupled with $c|_{y=H}$, i.e., c_w from the

solution of Eq. (25). This is done by considering a guess profile of $c(x)|_{y=H}$ and then calculating v_w and solving Eq. (25). The computed values of $c(x)|_{y=H}$ is compared with the guess values and iterated until convergence below a tolerance is attained.

Using the definition of mass transfer coefficient (k),

$$k(x) = \frac{D \left(\frac{\partial c}{\partial y} \right)_{y=H}}{c|_{y=H} - c_0} \quad (33)$$

Sherwood number (Sh) can be expressed as,

$$Sh(x) = \frac{k d_e}{D} = d_e \frac{(\partial c / \partial y)_{y=H}}{c_w - c_0} \quad (34)$$

where, d_e is the hydraulic diameter of the channel. In Eq. (34), the term $\left(\frac{\partial c}{\partial y} \right)_{y=H}$ is calculated from Eq. (28). The length averaged Sherwood number ($\overline{Sh_L}$) can thus be calculated as,

$$\overline{Sh_L} = \int_0^L Sh(x) dx \quad (35)$$

and the length averaged wall Peclet number ($\overline{Pe_w}$) is defined as,

$$\overline{Pe_w} = \frac{d_e}{D} \int_0^L v_w(x) dx \quad (36)$$

2.4 Computational technique

The sequence of the calculation steps in solving the present mathematical set of equations is illustrated by the algorithm in Fig. 2. An iterative scheme is employed to find

converged solutions of n_-^0, n_+^0 and ψ_C as depicted in the algorithm (Fig. 2). The boundary value ODE (Eq. 1) to evaluate ψ_C is solved using shooting method [44]. In the shooting technique, the boundary value ODE is reduced to an initial value problem by assuming a Dirichlet condition for $y = 0$ (ψ_C) in addition to Eq. (2a). The ODE is evaluated and shoots for the dirichlet condition at the other boundary ($\psi[y=H] = \zeta$). The relative difference is computed and if less than the tolerance, the process exits, else a new guess for ψ_C is defined following a secant method (interpolation) with the previous two iteration properties,

$$\psi_{Cg}^{i+1} = \psi_{Cg}^i - (\psi_{Cg}^i - \psi_{Cg}^{i-1}) / (m^i - m^{i-1}) \quad (37)$$

where i is the index of iteration and $m = (\psi[y=H] - \zeta) / \zeta$, is the relative error at the shooting boundary. The relative tolerance (ε_1) used for the convergence of ψ_C is set to 0.001. The starting value of ψ_{Cg} is the converged solution of the previous outer iteration loop.

However, for the case of convergence of n_-^0 and n_+^0 , a more sophisticated approach is considered. The inner loop is for convergence of n_-^0 and the tolerance criterion is ramped down proportional to the number of iterations of the outer loop (for convergence of n_+^0). The relative tolerance (ε_3) of the outer loop (for n_+^0) is preset at 0.01, whereas the relative tolerance for the inner loop (ε_2) is defined as $\frac{\varepsilon_3}{2} \left(1 + \frac{1}{n_{ind}} \right)$, where n_{ind} is the number of iterations of the outer loop. There is an under-relaxation factor of 0.3 for n_-^0 loop and 0.7 for convergence of n_+^0 . This is helpful in obtaining a global convergence for all variables over the local minima in the set of non-linear ODE's [45]. It is interesting to note that during the computation, the suitable choice of the guess values for n_-^0, n_+^0 and ψ_C for a particular κH actually accelerates the convergence. The speed of convergence depends on two factors,

namely, (i) difference of two subsequent κH should be less than 0.1; (ii) guess values for n_-^0, n_+^0 and ψ_C for a particular κH should be converged value at the preceding guess values for n_-^0, n_+^0 and ψ_C for a particular κH . The species convective-diffusive equation (23) is discretized using the first order upwind scheme. The mesh resolution near the porous interface is 10 times smaller than the scaled concentration boundary layer thickness ($\sim Sc^{1/3}$).

The following benchmarking analyses have been carried out and are reported here:

1. Grid independent study with the boundary element size corresponding to 20%, 15%, 10% and 5% of the approximate concentration boundary layer thickness was carried out for solution of the species transport equation (Eq. 25). For grid resolution of 10% and less, the mass continuity is less than 0.001, and is, therefore, accepted.
2. In the limit of macro-channels ($\kappa H \sim 100$), $\psi_c \rightarrow 0$ and $n_+^0 = n_-^0 = n^0$. Numerically, corresponding to $\kappa H = 100$, $\psi_c / \zeta \rightarrow 3.1 \times 10^{-05}$; $n_+^0 / n^0 = 0.0012$ and $n_-^0 / n^0 = 0.00058$.
3. In the asymptotic limit of $\zeta \rightarrow 0$, the velocity profile is perfectly parabolic in nature and is observed computationally, $(u - u_p)/u_p = 1.2 \times 10^{-4}$.
4. In the case of Debye-Hückel limit, for $\zeta = -5$ mV and -25 mV, the magnitude of $\overline{Sh_L}$ is comparable with the results in [33].
5. In the limit of $\zeta \rightarrow 0$ and $L_p \rightarrow 0$, expression of Sherwood number becomes $\overline{Sh_L} \sim 1.85 Re^{1/3}$, which is analogous to the result for impervious conduit [46].

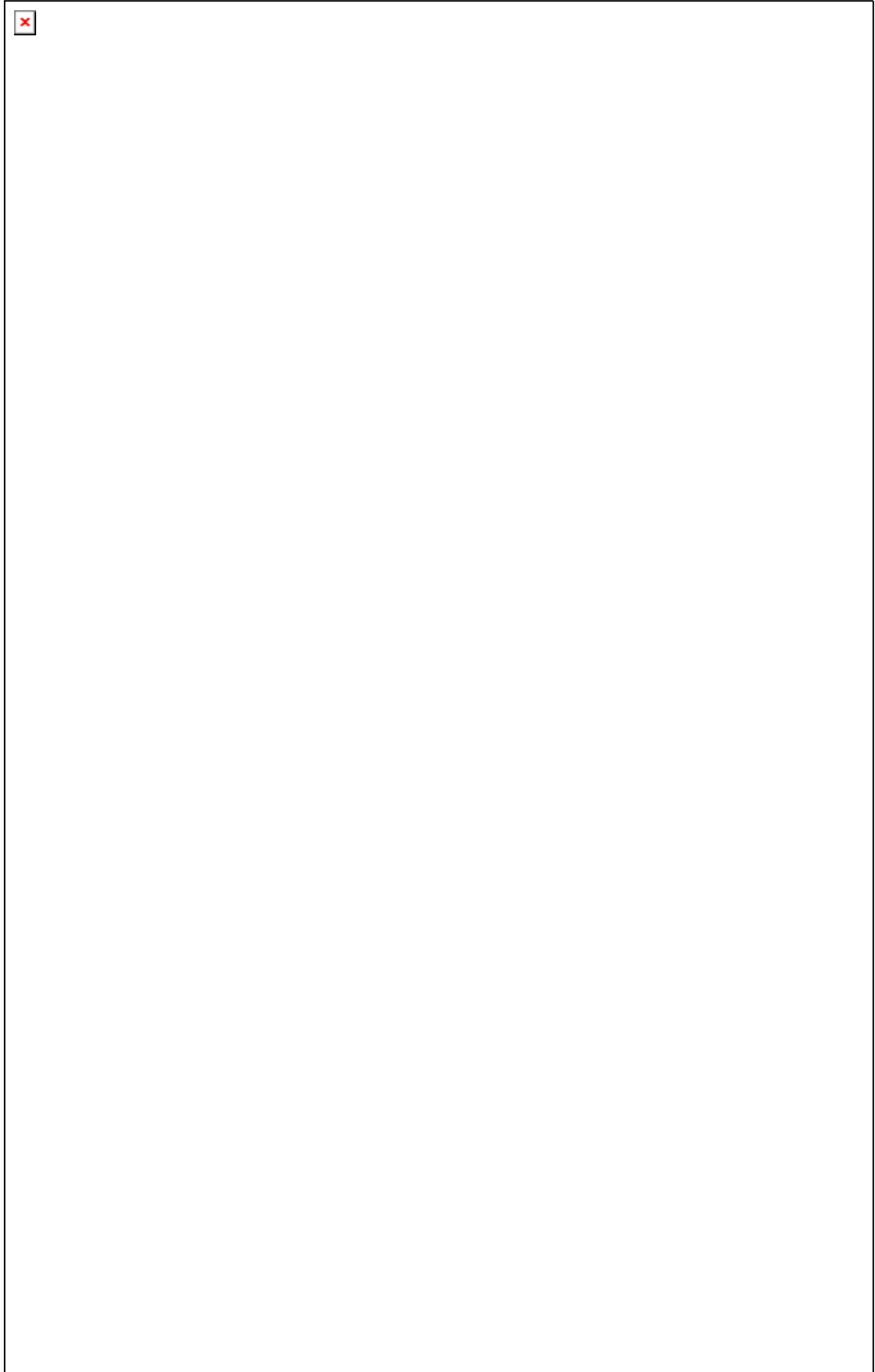


Fig. 2: Flow sheet describing the algorithm of the calculation steps in the present problem.

3.0 Results and Discussion

The potential distribution due to overlapping EDL is best represented by the magnitude of the centerline potential for different wall zeta potential, as shown in Fig. 3. The typical values of various parameters used for the simulation are given in Table 1. Selection of these parameters is in line with data available in literature [47, 48]. With increase in κH , the thickness of the EDL decreases causing the centerline potential to drop significantly. This effect is more prominent in case of lower wall zeta potential. The figure clearly shows that in case of $\zeta = -50$ mV, the EDL does not overlap beyond $\kappa H = 0.8$. The overall magnitude of the centerline potential (ψ_c) for $\zeta = -200$ mV does not reduce to zero for the studied range $0.1 < \kappa H < 1.5$. The anion and cation concentration profiles across the channels can be calculated using Eq. (20). The variation of the cation and anion concentration at the centre with κH is presented in Fig. 4. As in the present case of the negative wall potential the cation concentration decreases while the anion concentration increases. The relative magnitude of the concentration is determined by the pH , pH_{ZPC} and ΔpK_a of the solution. The cation concentration decreases with zeta potential which is just opposite in case of anion concentration. However, as observed in case of anion, the concentration is more in case of higher zeta potential at $\kappa H > 1.1$. These results clearly indicate that EDLs overlap at higher wall potential and lower κH .

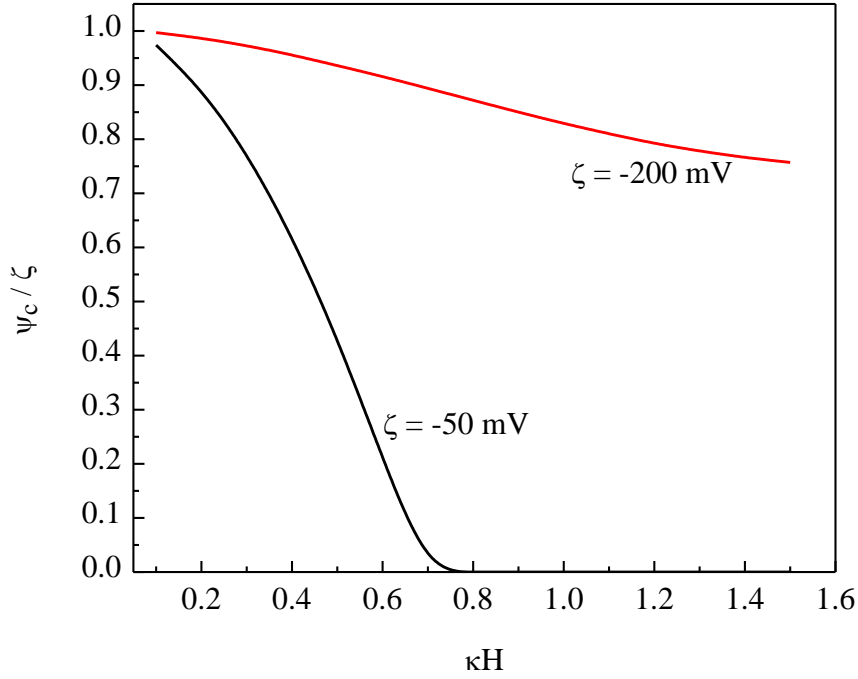


Fig. 3: Variation of the centerline potential with solution κH for different wall zeta potential

Table 1: Typical values of the physical parameters used in the simulation

Parameter	Value
Axial pressure gradient, p_x	2 MPa/m
Length of the microchannel, L	200 μm
Wall permeability, L_p	5×10^{-11} m/Pa.s
Channel half height, H	0.2 μm
Diffusivity of solute, D	1×10^{-12} m^2/s
Solute concentration, c_0	1 kg/m^3
Osmotic pressure coefficient, α_1	1000 Pa. $\text{m}^{3\alpha_2} . \text{kg}^{-\alpha_2}$
Osmotic pressure coefficient, α_2	1.5
Average pressure drop across the wall, ΔP_w	100 kPa

Real retention of the wall, R_r	0.9
Temperature, T	300 K
Ionic radius of the electrolyte, r_{ion}	1.5 Å
Viscosity of electrolyte solution, μ	1 mPa.s
Solution pH	6.2
Site density	5×10^{18} sites/m ²
pH_{zpc}	2.5
$\Delta p K_a$	10
Dielectric permittivity (ϵ_r)	80

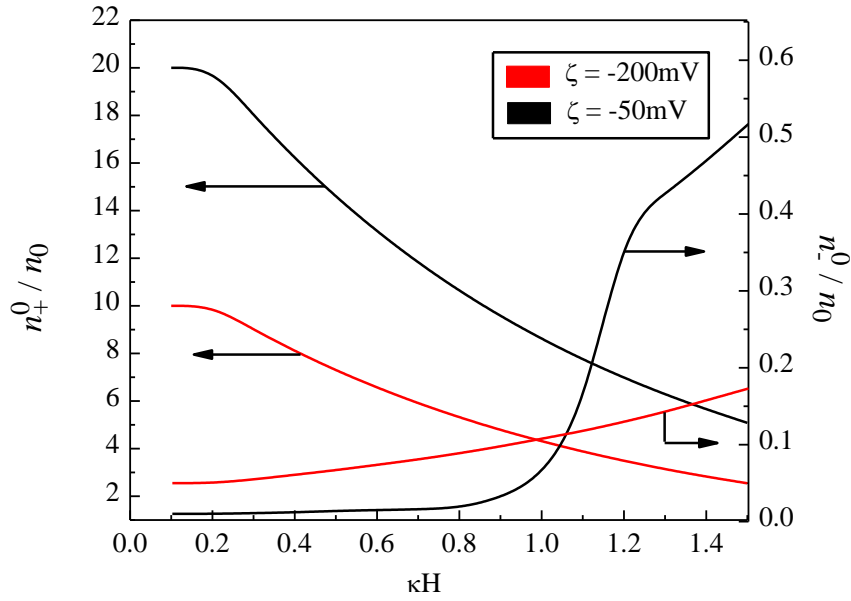


Fig. 4: Variation of the centerline cation and anion number concentration with solution κH .

The potential distribution and the effect of overlapping EDL across the channel cross section for different κH is illustrated in Fig. 5. It shows that the effect of the streaming potential spans the entire cross section for all values of $\kappa H < 0.8$ in the range of $|\zeta| > 50\text{mV}$.

The electrokinetic streaming potential is more at lower κH (curves 1 and 3) and at higher zeta

potential (curves 1 and 2). At these conditions, the centerline potential can be as high as 82% to 99% of wall potential indicating strong effects of EDL overlap. This figure clearly shows that inadequacy of Debye-Hückel approximation ($\sinh(\theta) \approx \theta$) in case of higher zeta potential. As discussed earlier, the corresponding anion and cation concentration distribution can be evaluated using Eq. (3).

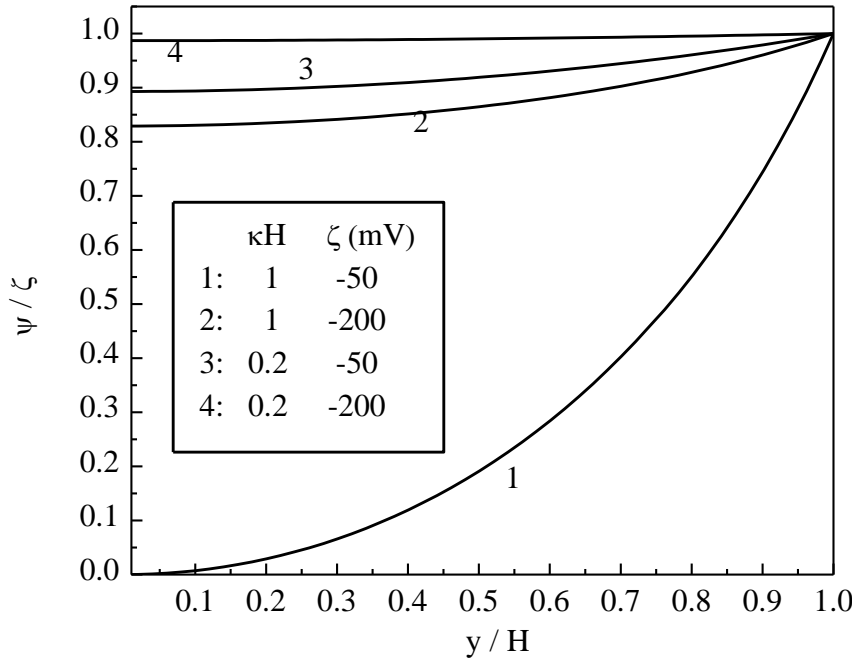


Fig. 5: Spatial profile of the potential distribution across the channel for different solution κH and wall zeta potential.

Variation of the streaming field as calculated from Eq. (23) is presented in Fig. 6. The streaming field increases with the wall zeta potential and decreases with solution κH . This fact can also be related from Fig. 5, since, the streaming potential distribution is more at higher κH and ζ . It can be mentioned here that the streaming field is dependent on the relative anion and cation concentration, which is unlike the case of lower wall potential [29]. As observed from this figure, the magnitude of the streaming field for lower zeta potential ($\zeta = -50$ mV) becomes constant beyond $\kappa H = 0.7$. This figure provides an insight to design

of and operation of such systems by selection of combination of wall potential, electrolyte concentration and channel dimension (H) in order to minimize the effect of streaming potential and hence electroviscous effects.

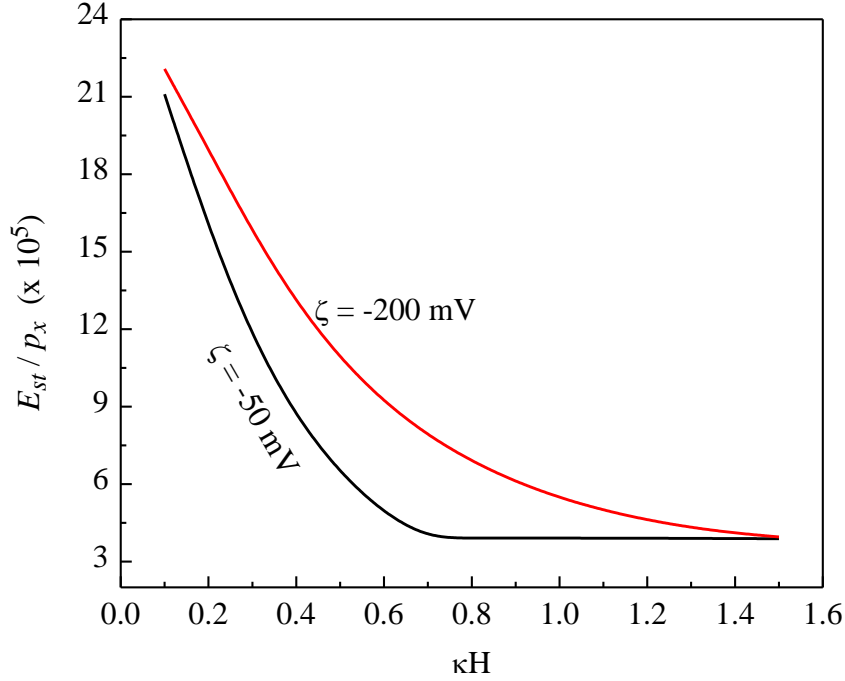


Fig. 6: Variation of the streaming electric field with solution κH for different wall zeta potential.

The velocity profile for different values of κH and ζ are presented in Fig. 7. The figure clearly shows that the overall flow velocity is affected by κH significantly. Comparing curve 2 and 3, it can be observed that the flow velocity is 1.7 times when κH is increased from 0.3 to 1.2. Interestingly, the effect of the wall zeta potential on the velocity is more at higher κH (comparing 3 and 4 with respect to 1 and 2), as the EDL is thin and the effect of potential distribution extends to the bulk of the channel. For example, at $\kappa H = 0.3$, the velocity changes by 65% whereas, it changes by more than 100% at $\kappa H = 1.2$, when $|\zeta|$ is increased from 50 to 200 mV. At higher zeta potential, the potential distribution across the channel is more due to the overlapping of the double layer. As a result, the velocity

distribution is affected more by the increased zeta potential. Depending on the magnitude of the system parameters, there can be a situation when the net velocity becomes zero [49]. However, such a situation is not attained with the present parameter combination.

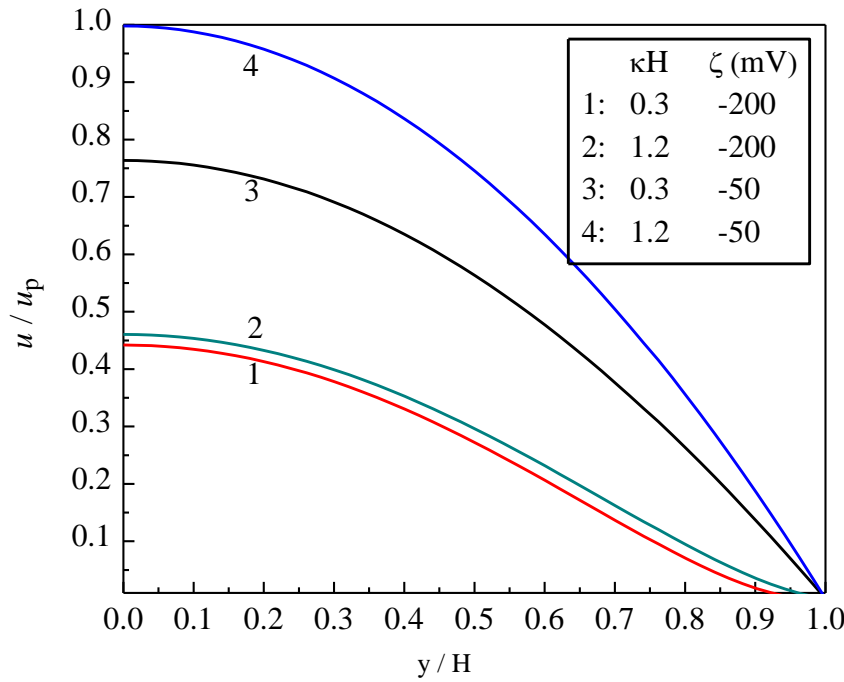


Fig. 7: Velocity profile across the channel for different values of solution κH and wall zeta potential.

The effect of the solution κH on the electroviscous effect and Sherwood number for different values of surface potential is presented in Fig. 8. The relative apparent viscosity

$\left(\frac{\mu_{app}}{\mu} \right)$ is defined as the ratio of the total volumetric flowrate in case of Poiseuille flow to

the flow due to electrokinetic effects mentioned in Eq. (17), $2u_p H / \int_{-H}^H u(y) dy$. The rise in

the apparent viscosity of the solution can be more than 3.5 times of the solution viscosity for high zeta potential and low κH . It should be noted that the maximum impact of electroviscous phenomena is observed when the Debye layer thickness is more than the

channel width ($\kappa H < 1$). This figure also quantifies the range of κH , when electroviscous effects are prominent. As expected, the range of κH increases with the magnitude of ζ under electroviscous effects. For example, the range of κH (when $\frac{\mu_{app}}{\mu} > 1.1$) increases from 0.7 to 1.1 as $|\zeta|$ increases from 50 to 200 mV. The drop in the Sherwood number as observed in the figure is attributed due to the electroviscous effect resulting in reduction of the overall velocity profile. Minimum Sherwood number is obtained for κH values corresponding to the maximum apparent viscosity, as evident from Fig. 8(a). As observed from Fig. 8(b), the minimum Sherwood number is obtained at $\kappa H = 0.3$ for $\zeta = -50$ mV, while it is at $\kappa H = 0.5$ for $\zeta = -200$ mV. Also, the minimum value is lower for higher zeta potential. In case of lower zeta potential, the effect of the streaming field diminishes at lower κH . Hence, the magnitude of $\overline{Sh_L}$ approaches asymptotic value in case of mass transport in rectangular channel due to poiseuille flow only at lower κH ($\zeta = -50$ mV), compared to the case of $\zeta = -200$ mV. The locus of minimum $\overline{Sh_L}$ for different κH and ζ is presented in the inset of Fig. 8(b). This figure indicates that for a given zeta potential of the wall, κH should be above the curve (inset), in order to have significant mass transport. This curve provides a design basis of selection of κH and wall potential for substantial mass transport during separation of neutral macrosolute in such microchannel with porous walls.

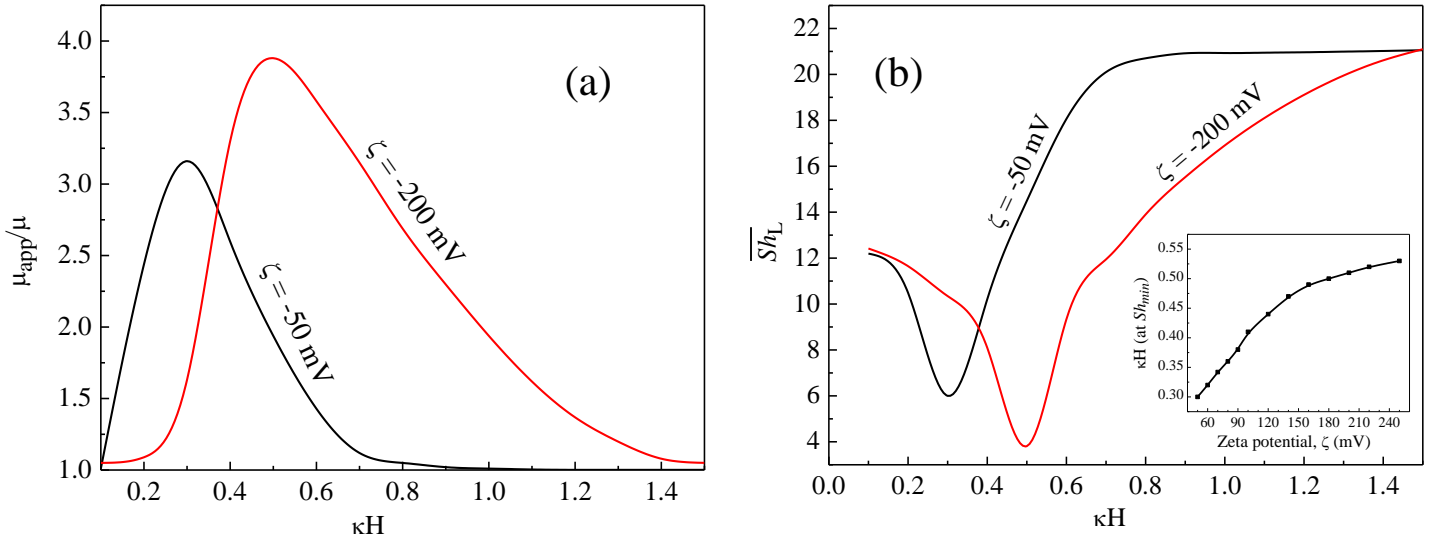


Fig. 8: (a) Rise of the apparent solution viscosity with solution κH and (b) Variation of the length averaged Sherwood number for different values of solution κH (inset: phase space plot of κH with ζ corresponding to Sherwood minima).

The system performance is quantified in terms of the permeation rate and permeate concentration. The effect of the solution κH on length averaged wall Pe number (\overline{Pe}_w) is shown in Fig. 9. The wall Pe signifies the permeation rate and can be estimated experimentally. Similar to the case of \overline{Sh}_L profile, \overline{Pe}_w decreases for higher zeta potential. This is because the electroviscous effect becomes more prominent with the surface potential, as shown in Fig. 8(a). Due to EDL overlap, the minima for \overline{Pe}_w is attained at lower κH for low zeta potential ($\zeta = -50$ mV). The permeate concentration for different wall zeta potential is represented in Fig. 10. The concentration polarization of the macrosolute at the wall is increased due to apparent rise in viscosity by the electroviscous phenomenon (described by Fig. 8a). As the solute surface concentration over the porous wall increases, the permeate concentration also increases as shown in the inset of this figure. The maximum concentration polarization of the macrosolute occurs at $\kappa H = 0.3$ for $\zeta = -50$ mV and at $\kappa H = 0.5$ for $\zeta = -200$ mV, for the given set of parameters as described in Table 1. One can

select the solution κH for a given wall potential to realize the extent of permeation quality of the macrosolute. The trend for the permeate concentration (C_p) is just in accordance to the understandings of the previous figure.

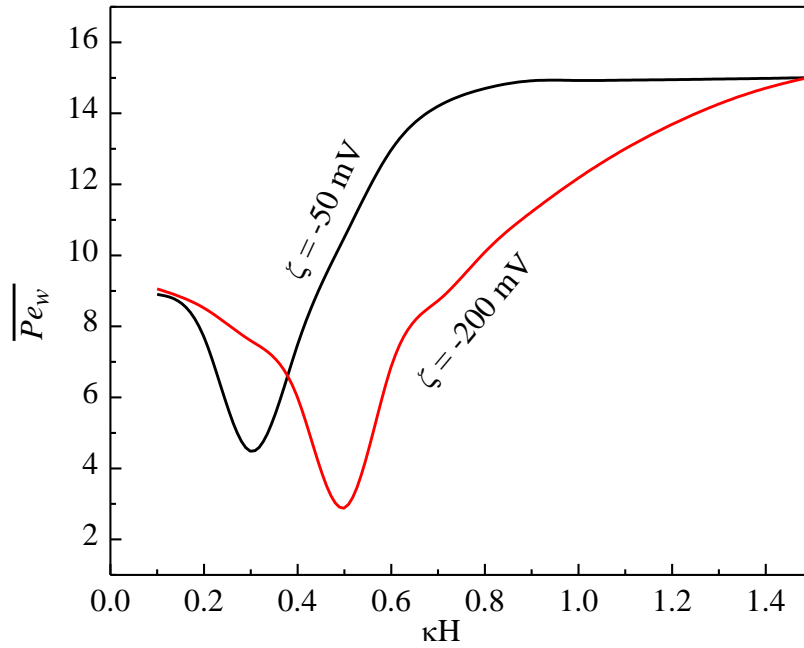


Fig. 9: Variation of the length averaged wall Peclet number for different values of solution κH .

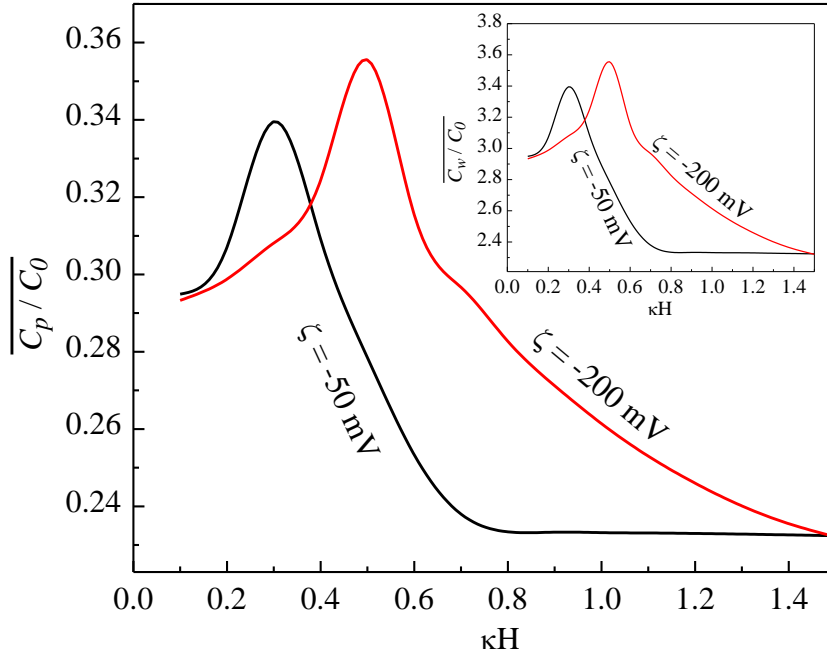


Fig. 10: Variation of the length averaged macrosolute concentration in permeate for different values of solution κH (inset: Profiles of wall macrosolute concentration)

4.0 Conclusion

The pressure driven flow through microchannel with porous wall under high surface potential and overlapping EDL is quantified in this study. The major conclusions derived from this study are presented below:

- (i) Streaming field and the overlapping phenomena is significant at κH less than 1. The EDL overlaps for $\kappa H < 0.7$ at $\zeta = -50 \text{ mV}$ and $\kappa H < 3.6$ at $\zeta = -200 \text{ mV}$.
- (ii) The potential distribution and the streaming field have strong influence on the velocity profile. The overall velocity is almost half of the pure poiseuille velocity for zeta potential 200 mV in aqueous medium.
- (iii) Mass transfer is minimum due to the electroviscous effects. Minimum Sherwood number decreases by 40% when zeta potential ($|\zeta|$) is increased from 50 mV to 200 mV. Also the

minimum Sherwood number is attained at $\kappa H = 0.3$ for $\zeta = -50 \text{ mV}$ and $\kappa H = 1.2$ for $\zeta = -200 \text{ mV}$.

(iv) The minimum wall permeation decreases ($\overline{Pe_w}$) from 4.2 to 3.1 (25%) as $|\zeta|$ is increases from 50 to 200 mV.

(v) The solute concentration in the permeate increases due to concentration polarization and reduction in overall velocity due to the streaming field effect. The magnitude of solute concentration is dependent on the real retention of the wall.

(vi) In the case of large zeta potential, the effect of the ion adsorption to channel walls is significant [50], which is not included in the present model, as stated in one of the assumptions. However, incorporation of such effects can be taken up as an improvement to the existing analysis.

5.0 Nomenclature

c	Concentration of the macrosolute, kg/m^3
c_0	Inlet concentration of the macrosolute, kg/m^3
c_p	Concentration of the permeate, kg/m^3
c_p^*	Non-dimensional permeate concentration of the macrosolute, c_p/c_0
$\overline{c_p^*}$	Length averaged non-dimensional permeate concentration of the macrosolute
c_w	Concentration of macrosolute over the porous wall, kg/m^3
c_w^*	Non-dimensional wall concentration of the macrosolute, c_w/c_0
$\overline{c_w^*}$	Length averaged non-dimensional wall concentration of the macrosolute
D	Diffusivity of the macrosolute, m^2/s
d_e	Hydraulic diameter of the channel, m
e	Charge of an electron, C
E_{st}	Streaming field, V/m
H	Half height of the channel, m
I_{cond}	Conduction current, A
I_{ionic}	Total ionic current, A
I_{str}	Streaming current, A
k	Mass transfer coefficient, m/s
k_b	Boltzmann constant, $\text{m}^2 \text{ kg. s}^{-2} \text{ K}^{-1}$
K_W	Dissociation constant of water, 10^{-14}
L	Length of the microchannel, m
L_p	Permeability of the porous wall, Pa.s
m	Relative error in shooting technique, refer to Eq. (37)
n^+	Number concentration of the cation, numbers/mol

n_+^0	Cation number concentration at the center of the channel, number/mol
n_-	Number concentration of the anion, numbers/mol
n_-^0	Anion number concentration at the center of the channel, number/mol
n_{Cl^-}	Number concentration of the chloride ion in solution, numbers/mol
N_d	Number of water molecules dissociated into H_3O^+ and OH^-
$n_{H_3O^+}$	Number concentration of the hydronium ion in solution, numbers/mol
$n_{H_3O^+}^0$	Number concentration of hydronium ion at the channel center, numbers/mol
$\overline{n_{H_3O^+}}$	Average number concentration of the hydronium ion in solution, numbers/mol
n_{K^+}	Number concentration of the potassium ion in solution, numbers/mol
n_{OH^-}	Number concentration of the hydroxide ion in solution, numbers/mol
$n_{OH^-}^0$	Number concentration of hydroxide ion at the channel center, numbers/mol
$\overline{n_{OH^-}}$	Average number concentration of the hydroxide ion in solution, numbers/mol
N_s	Density of the charged surface, sites/m ³
Pe_w	Wall Peclet number
$\overline{Pe_w}$	Length averaged wall Peclet number
pH	Negative logarithm (base 10) of H_3O^+ molar concentration in the solution
pH_{ZPC}	pH of the solution at which the charged surface is neutral
p_x	Axial pressure gradient, Pa/m
r^\pm	Radius of the cation or anion, m
R_r	Real retention of the porous wall
Sh	Sherwood number

\overline{Sh}_L	Length averaged Sherwood number
T	Temperature, K
u	Overall velocity profile, m/s
u_{cond}^{\pm}	Conduction velocities of cation and anion, m/s
u_p	Average cross sectional velocity ($= p_x H^2 / 3\mu$), m/s
v_w	Transverse velocity (quantified as permeation rate), m/s
x	Axial co-ordinate, m
y	Vertical co-ordinate, m
z	Valence of the cation or anion in case of symmetric electrolyte

Greek Symbols

α	Non-dimensional term defined in Eq. (4), $\alpha = \frac{ze\psi}{k_B T}$
α_1, α_2	Co-efficient for computing osmotic pressure using power law, (unit of α_1 is $\text{Pa.m}^{3\alpha_2}.\text{kg}^{-3\alpha_2}$)
δ	Parameter defined in Eq. 6
ϵ_0	Permittivity of vacuum, $8.854 \times 10^{-12} \text{ CV}^{-1}.\text{m}^{-1}$
ϵ_r	Relative permittivity of the electrolyte medium
$\epsilon_{1, 2, 3}$	Relative tolerance for convergence of ψ_C, n_-^0 and n_+^0
$\Delta\pi$	Osmotic pressure difference between wall and permeate side, Pa
ΔP_w	Gauge Pressure inside the channel, Pa
ΔpK	Difference of the dissociation constants
κ	Inverse of Debye layer thickness, m^{-1}
μ	Solution viscosity, Pa.s

μ_{app}	Apparent solution viscosity due to electroviscous phenomena, Pa.s
π	Osmotic pressure of solution, Pa
σ_0	Surface charge density, C/m ³
ψ	EDL potential distribution, V
ψ_C	EDL potential at the center of the channel, V
ψ_N^*	Non-dimensional Nernst potential, ψ_N/ζ
ζ	Wall zeta potential, V

References

- [1] Whitesides GM. The origins and the future of microfluidics. *Nature*. 2006; 442: 368-373.
- [2] Li D. *Electrokinetics in Microfluidics*. London: Elsevier, 2004.
- [3] Brandner JJ, Anurjew E, Bohn L, Hansjosten E, Henning T, Schygulla U, Wenka A, Schubert K. Concepts and realization of microstructure heat exchangers for enhanced heat transfer. *Experimental Thermal Fluid Science*. 2006; 30: 801-809.
- [4] Goodson KE, Chen CH, Huber DE, Jiang L, Kenny TW, Koo JM, Laser DJ, Mikkelsen JC, Santiago JG, Wang ENY, Zeung S, Zhang L. Electroosmotic microchannel cooling system. US patent. 2005; 6942018.
- [5] Damean N, Regtien PPL, Elwenspoek M. Heat transfer in a MEMS for microfluidics. *Sensors and Actuators A*. 2003; 105: 137-149.
- [6] Pohar A, Plazl I. Laminar to turbulent transition and heat transfer in a microreactor: mathematical modeling and experiments. *Industrial & Engineering Chemistry Research*. 2008; 47: 7447–7455.

- [7] Banga AK, Chien YW. Iontophoretic delivery of drugs: fundamentals, developments and biomedical applications. *Journal of Controlled Release*. 1988; 7: 1-24.
- [8] Arora A, Prausnitz MR, Mitragotri S. Micro-scale devices for transdermal drug delivery. *International Journal of Pharmaceutics*. 2008; 364: 227-236.
- [9] Karimi G, Li X. Electroosmotic flow through polymer electrolyte membranes in PEM fuel cells. *Journal of Power Sources*. 2005; 140: 1-11.
- [10] Matos MA, White LR, Tilton RD. Electroosmotically enhanced mass transfer through polyacrylamide gels. *Journal of Colloid and Interface Science*. 2006; 300: 429-436.
- [11] Dutta D. Electroosmotic transport through rectangular channels with small zeta potentials. *Journal of Colloid and Interface Science*. 2007; 315: 740–746.
- [12] Sadeghi A, Amini Y, Saidi MS, Chakraborty S. Numerical modeling of surface reaction kinetics in electrokinetically actuated microfluidic devices. *Analytica Chimica Acta*. 2014; 838: 64–75.
- [13] Subramaniam K, Chakraborty S. A semi-analytical model for species transport in combined electroosmotic and pressure driven microflows with surface adsorption–desorption reactions. *Microfluidics and Nanofluidics*. 2011; 10: 821–829.
- [14] Li D. Electro-viscous effects on pressure-driven liquid flow in microchannels. *Colloids and Surfaces A: Physiochemical and Engineering Aspects*. 2001; 195: 35-57.
- [15] Ren CL, Li D. Electroviscous effects on pressure-driven flow of dilute electrolyte solutions in small microchannels. *Journal of Colloid and Interface Science*. 2004; 274: 319-330.
- [16] Tang GH, Ye PX, Tao WQ. Electroviscous effect on non-Newtonian fluid flow in microchannels. *Journal of Non-Newtonian Fluid Mechanics*. 2010; 155: 435-440.
- [17] Masliyah JH, Bhattacharjee S. *Electrokinetic and Colloid Transport Phenomena*. New Jersey: Wiley, 2006.

- [18] Wang M, Chang CC, Yang RJJ. Electroviscous effects in nanofluidic channels. *Chemical Physics*. 2010; 132: 024701.
- [19] Yuan Z, Garcia AL, Lopez GP, Petsev DN. Electrokinetic transport and separations in fluidic nanochannels. *Electrophoresis*. 2007; 28: 595–610.
- [20] Molla SH, Bhattacharjee S. Dielectrophoretic levitation in the presence of shear flow: Implications for colloidal fouling of filtration membranes. *Langmuir*. 2007; 23: 10618-10627.
- [21] Breuer K. *Microscale Diagnostic Techniques*. Berlin: Springer-Verlag, 2005.
- [22] Xuan X. Streaming potential effects on solute dispersion in nanochannels. *Analytical Chemistry*. 2007; 79: 7928-7932.
- [23] Das S, Chakraborty S. Effect of Conductivity Variations within the Electric Double Layer on the Streaming Potential Estimation in Narrow Fluidic Confinements. *Langmuir*. 2010; 26: 11589-11596.
- [24] Das S, Chakraborty S. Influence of Streaming Potential on the Transport and Separation of Charged Spherical Solutes in Nanochannels Subjected to Particle–Wall Interactions. *Langmuir*. 2009; 25: 9863-9872.
- [25] Vennela N, Mondal S, Bhattacharjee S, De S. Sherwood number in flow through parallel porous plates (Microchannel) due to pressure and electroosmotic flow. *AIChE Journal*. 2012; 58: 1693-1703.
- [26] Vennela N., Bhattacharjee S, De S. Sherwood number in porous microtube due to combined pressure and electroosmotically driven flow. *Chemical Engineering Science*. 2011; 66: 6515-6524.
- [27] Mondal S, De S. Mass transport in a porous microchannel for non-Newtonian fluid with electrokinetic effects. *Electrophoresis*. 2013; 34: 668–673.

- [28] Mondal S, De S. Effects of non-Newtonian power law rheology on mass transport of a neutral solute for electro-osmotic flow in a porous microtube. *Biomicrofluidics*. 2013; 7: 044113.
- [29] Dejam M, Hassanzadeh H, Chen Z. Shear dispersion in combined pressure-driven and electro-osmotic flows in a channel with porous walls. *Chemical Engineering Science*. 2015; 137: 2015-215.
- [30] Dejam M, Hassanzadeh H, Chen Z. Shear Dispersion in Combined Pressure-Driven and Electro-Osmotic Flows in a Capillary Tube with a Porous Wall. *AIChE Journal*. 2015; 61: 3981-3995.
- [31] Zhao G, Jian Y, Li F. Streaming potential and heat transfer of nanofluids in parallel plate microchannels. *Colloids & Surfaces A: Physiochemical and Engineering Aspects*. 2016; 498: 239-247.
- [32] Chen G, Das S. Streaming potential and electroviscous effects in soft nanochannels beyond Debye–Hückel linearization. *Journal of Colloid and Interface Science*. 2015; 445: 357-363
- [33] Mondal S, De S. Mass transfer of a neutral solute in porous microchannel under streaming potential. *Electrophoresis*. 2014; 35 : 681–690.
- [34] Healy TH, White LR. Ionizable surface group models of aqueous interfaces. *Advanced in Colloid and Interface Science*. 1978; 9: 303-345.
- [35] Qu W, Li D. A Model for Overlapped EDL Fields. *Journal of Colloid and Interface Science*. 2000 ; 224 : 397-407.
- [36] Yang C, Li D, Masliyah JH. Modeling forced liquid convection in rectangular microchannels with electrokinetic effects. *International Journal of Heat and Mass Transfer*. 1998; 30: 4229-4249.

- [37] Mondal M, Misra RP, De S. Combined electroosmotic and pressure driven flow in a microchannel at high zeta potential and overlapping electrical double layer. *International Journal of Thermal Sciences*. 2014 ; 86 : 48-59.
- [38] De S, Bhattacharjee S, Sharma A, Bhattacharya PK. Generalized integral and similarity solutions of the concentration profiles for osmotic pressure controlled ultrafiltration. *Journal of Membrane Science*. 1997; 130: 99-121.
- [39] Nield DA, Bejan A. *Convection in Porous Media*. New York: Springer, 2013.
- [40] Kedem O, Katchalsky A. A physical interpretation of the phenomenological coefficients of membrane permeability. *Journal of General Physiology*. 1961; 45: 143–171.
- [41] Vilker VL, Colton CK, Smith KA. The osmotic pressure of concentrated protein solutions: Effect of concentration and pH in saline solutions of bovine serum albumin. *Journal of Colloid and Interface Science*. 1981; 79: 548–566.
- [42] Perry JD. Concentration Dependence of Osmotic Pressure in the Semidilute Range. *Macromolecules*. 1980; 13: 1719–1720.
- [43] Opong WS, Zydney AL. Diffusive and convective protein transport through asymmetric membranes. *AIChE Journal*. 1991; 37: 1497-1510.
- [44] Roberts SM, Shipman JS. *Two-point boundary value problems: shooting methods*. Elsevier Publishing Company; 1972.
- [45] Ortega JM, Rheinboldt WC. *Iterative solution of Nonlinear Equations in Several Variables*. (SIAM ed.) 2000; Academic Press: New York
- [46] De S, Bhattacharya PK. Prediction of mass-transfer coefficient with suction in the applications of reverse osmosis and ultrafiltration. *Journal of Membrane Science*. 1997; 128: 119-31.

- [47] Sisan TB, Lichter S. The end of nanochannels. *Microfluidics and Nanofluidics*. 2011; 11: 787–791
- [48] Yang RJ, Fu LM, Lin YC. Electroosmotic Flow in Microchannels. *Journal of Colloid and Interface Science*. 2001; 239: 98-105.
- [49] Das S, Guha A, Mitra SK. Exploring new scaling regimes for streaming potential and electroviscous effects in a nanocapillary with overlapping Electric Double Layers. *Analytica Chimica Acta*. 2013; 804: 159-166.
- [50] Borukhov I, Andelman D, Orland H. Adsorption of large ions from an electrolyte solution: a modified Poisson–Boltzmann equation. *Electrochimica Acta*. 2000; 46: 221-229.